MINERALOGICAL MAGAZINE, JUNE 1984, VOL. 48, PP. 181-93

Mineral chemistry of coexisting phases from shonkinitic rocks, Salem, Tamil Nadu, India

C. R. L. FRIEND

Department of Geology and Physical Sciences, Oxford Polytechnic, Oxford, OX3 0BP, UK

AND

A. S. JANARDHAN

Department of Geology, University of Mysore, Manasagangotri, Mysore 570006, India

ABSTRACT. Gabbroic-textured shonkinitic rocks of unknown age cut deformed Archaean dunites and peridotites in the area immediately north of Salem. Magnesite formation post-dates their intrusion. The location of these rocks and the magnesite is thought to be controlled by the intersection of two major basement lineaments. A sequence of crystallization of the minerals and rocks from early undersaturated to late oversaturated rocks is established. Compositions of the coexisting mineral phases are reported here for the first time. Clinopyroxenes, which are relatively unevolved, commonly coexist with olivine (chrysolite) and sanidine. Bronzite, often intergrown with magnetite and green spinel, is occasionally present. In the most undersaturated rocks nepheline–sanidine fingerprint intergrowths occur, whilst perthitic sanidine, albitic plagioclase, and quartz are present in over-saturated rocks. Late in the crystallization sequence, in oversaturated rocks, P_{H_2O} appears to have increased allowing the formation of amphibole as well as clinopyroxene.

IN the southern portion of the Indian shield there is a variety of igneous bodies intruded after the main period of Archaean metamorphic evolution. These bodies are essentially post-tectonic and have a wide range of composition, from relatively common granitic lithologies through to ultrabasic compositions and rarer, more exotic bodies such as carbonatites, syenites, and shonkinites.

Shonkinitic rocks were first reported to occur amongst a group of dunites and peridotites near Salem, Tamil Nadu (fig. 1) by Ramanathan (1954). Later, a more detailed petrographic account based upon that earlier work, appeared (Naidu, 1963). More recently, another contribution dealing briefly with the shonkinitic rocks has been published (Murthy, 1979). These authors have related the shonkinitic rocks to the ultrabasic rocks in which they are found (fig. 1). In the light of the new petrographic and mineralogical data presented here, this is considered an unlikely interpretation. We consider that whilst spatially related they are magmatically separate.

The shonkinitic rocks are of unknown age but, since they are undeformed, clearly post-date all of the Archaean metamorphic evolution of the basement rocks—Peninsular gneisses—which they intrude. They also intrude a group of dunitic and peridotitic rocks (fig. 1) which again are of unknown age. Whilst these ultrabasic rocks possess a deformational fabric, they may be separated from the basement rocks since they cut the structures in the gneisses (Naidu, 1963). The deformational textures include a foliation on an outcrop scale whilst, in thin section, mortar texture and strain lamellae are common and kink bands are widespread throughout the olivines of the dunites, together with advanced serpentinization associated with the peridotites. We interpret this deformation to be synchronous with the time of emplacement of these rocks into the crust. The shonkinitic rocks cut these structures, evidence for which is the occurrence of deformed and foliated xenoliths of dunite in the shonkinites, though direct contacts are difficult to observe because of the development of magnesite. However, because of the lack of any deformational textures in the shonkinitic rocks it is considered unlikely that the magmas giving rise to the ultrabasic and the shonkinitic rocks were related.

Murthy (1979) relates the location of the ultrabasic rocks and the cross-cutting shonkinites to an intersection of two major fault systems trending NE–SW and NW–SE. He notes that strung out along the NE–SW trending system are other ultrabasic bodies which, he suggests, are all related. This intersection of major deep-seated structures has been discussed by Drury and Holt (1980) who consider the NE trending structure to be an

extension of the Proterozoic Moyar–Bhavani shear. Such a structure may well be the controlling factor in the location of the ultrabasic rocks at Salem and was probably responsible for allowing the ingress of fluids which gave rise to the formation of the magnesite. Since there is good field evidence to place the shonkinites between the ultrabasic rocks and the magnesite it is plausible that their evolution was controlled by the same structure. Magnesite veins are developed very sparsely in the shonkinitic rocks and those present are of poor quality, being very siliceous and of no economic value, the areas of shonkinite are therefore being covered and infilled by spoil.

Petrography. The observations of this study significantly extend the range of compositions previously reported and the minerals involved (Ramanathan, 1954; Naidu, 1963). Texturally, all the samples are coarse-grained and vary from gabbroic to more ultramafic types (Table I).

Naidu (1963) summarized the rocks as comprising three groups which are characterized by sanidine or orthoclase cryptoperthite, either without feldspathoid or coexisting with either nepheline or leucite and pseudoleucite. This grouping is extended here to include two new types, one which contains plagioclase, alkali feldspar, and quartz and the other containing no felsic phases (Table I). Nepheline has been found in one sample (SN103) as well as in complex association with potassium feldspar. However, the report of microcline in these rocks (Murthy, 1979) has not been duplicated. The felsic minerals in these rocks are thus extremely important since they indicate a range in composition from silica undersaturated, feldspathoidal types to over saturated quartz-bearing types. The modal analyses of the rocks examined are presented in Table I.

Using the nomenclature of Streckeisen (1976) the gabbroic-textured rocks are alkali syenites, whilst the ultramafic types are olivine websterites and olivine-hornblende pyroxenites. On a more detailed basis, using the classification given by Sørensen (1974), rocks with $< 10\%$ plagioclase, 0–5% quartz, and 0–10% feldspathoids may be called shonkinites or alkali melasyenites. However, when compared with the type shonkinites (Hurlbut and Griggs, 1939; Nash and Wilkinson, 1970) these rocks differ slightly, since the olivine is more forsteritic.

In SN103 subhedral nepheline occurs scattered

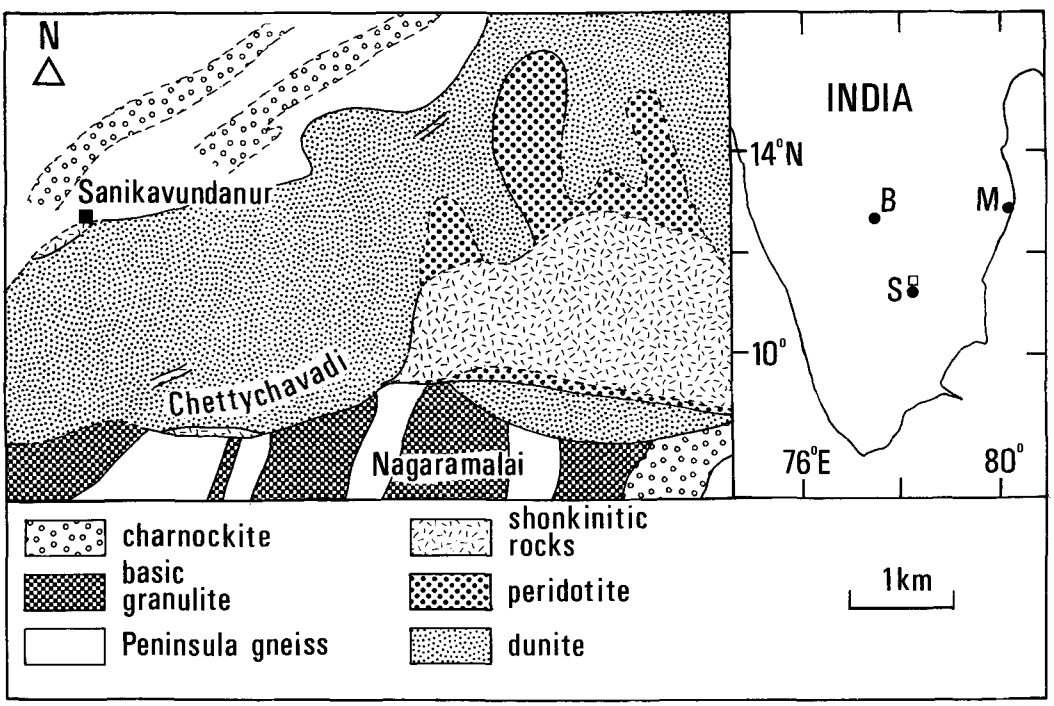

FIG. 1. Location of the Chalk Hills area, Salem, Tamil Nadu. Inset map of southern India: S = Salem; B = Bangalore; M = Madras. Geological sketch-map of the geology of the Chalk Hills magnesite area, about 5 km north of Salem, showing the location of the shonkinitic rocks. Map redrawn from Naidu (1963) and modified with data from the Dalmia Magnesite Mining Corporation.

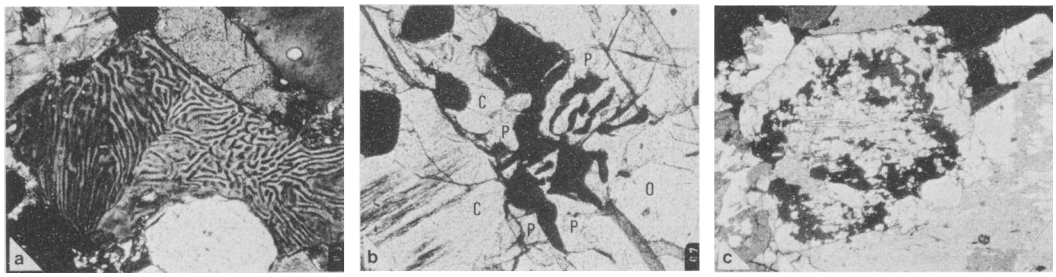

FIG. 2. (*a*) Complex fingerprint intergrowth of nepheline and K-feldspar, XPL (SN103). Width of photograph 0.5 mm. (*b*) Symplectic intergrowth of bronzite, magnetite, and green spinel, PPL (SN68). Width of photograph 1.0 mm, O = olivine, C = clinopyroxene, P = bronzite. (*c*) Relationships of amphibole and clinopyroxene showing an annular zone of amphibole (*in extinction*) contained within euhedral clinopyroxene, XPL (SN15). Width of photograph 1.5 mm.

amongst the potassium feldspar and frequently associated with a complex fingerprint intergrowth texture (fig. 2*a*). This texture (also present in samples D16 and SN105) cannot be resolved optically, but from microprobe analysis (see below) may be interpreted as an intergrowth of nepheline and potassium feldspar. This structure is similar to some of the intergrowths similarly interpreted by Naidu (1963) and to those reported from other alkaline rocks (e.g. Davidson, 1970; Mitchell and Platt, 1979). These samples are, therefore, considered to be the least-evolved in the sequence identified in the current study (Table I).

The feldspars are texturally complex and occur in several different forms. Generally, with the exception of the ultramafic samples, the most commonly occurring form is euhedral prisms of carlsbad twinned potassium feldspar which may have slightly undulose extinction. Additionally in these rocks the same composition feldspar may occur as anhedral to subhedral interstitial aggregates. For chemical reasons (see below) they are considered to be sanidines (cf. Naidu, 1963). In the ultramafic samples, potassium feldspar forms less than 5% (Table I) and is entirely interstitial. Of these samples SN66 and SN106 are interesting as they texturally

TABLE I. Modes of shonkinitc rocks from Salem

	Olv	Opx	Cpx	Amp	Phl	Kf	Ne+	Qtz	Pl	Op+	Ap+	Ep	No.
SN103	18.7	-	26.7	-	3.5	37.6	10.9	-	-	1.8	1.2	-	2000
D16	26.0	-	43.7	-	1.5	27.4	0.8	-	-	0.5	0.2	-	4000
SN101	22.5	tr	40.2	-	2.6	31.9	0.8	-	-	0.8	1.0	-	3000
SN107	52.9	0.7	45.5	-	0.5	-	-	-	-	0.5	-	-	1000
D12	41.2	-	50.7	-	2.3	4.1	-	-	-	1.7	tr	-	1000
SN105	39.2	-	56.1	-	1.0	2.8	-	-	-	0.9	tr	-	2000
SN66	28.3	0.8	55.9	12.1	0.8	-	-	-	-	0.9	1.2	-	1000
SN104	21.4	tr	74.8	-	0.4	2.7	-	-	-	0.5	-	-	2000
SN106	17.1	0.3	72.7	6.6	-	-	-	-	-	3.4	-	-	1000
SN110	31.3	-	49.9	-	2.1	23.3	-	-	-	0.3	0.2	-	2000
SN8	29.9	-	46.4	-	2.3	21.1	-	-	-	1.7	tr	-	1000
SN109	28.4	-	39.1	-	1.6	30.5	-	-	-	0.2	0.2	-	1000
SN75	26.6	0.8	49.9	-	0.3	22.0	-	-	-	0.4	tr	-	1000
SN64	25.6	-	51.2	-	0.9	22.0	-	-	-	0.4	0.2	-	1000
SN65	23.7	-	47.7	-	0.8	27.5	-	-	-	0.3	0.1	-	1000
SN68	23.1	0.2	52.3	-	0.2	32.8	-	-	-	0.4	tr	-	1000
SN67	20.3	0.2	47.1	-	0.5	31.6	-	-	-	0.2	0.1	-	1000
SN13	15.7	-	41.9	-	2.2	39.3	-	-	-	0.7	0.2	-	3000
SN15	-	-	25.2	55.2	1.8	10.7	-	0.9	4.7	0.2	0.1	1.2	3000

tr = trace, below 0.1%

Ne+ = Nepheline plus nepheline–K-feldspar intergrowths

Op+ = Opaques plus pleonaste spinel

Ap+ = Apatite plus calcite

resemble cumulates. SN15 is most complex sample and there are four optically and texturally different types of feldspar recognized: (i) interstital, non-perthitic, potassium feldspar, present in small amounts and resembling that found in the other rocks; (ii) a patchy micro-perthite—bead or interlocking perthite (Deer *et al.*, 1963)—which is usually found as irregular plates; (iii) large poikilitic plates of polysynthetically twinned albitic plagioclase with antiperthite; (iv) non-perthitic potassium feldspars which are intergrown with quartz. Occurring as scattered crystals in these plates are a few anhedral grains of epidote.

Since quartz is present in this sample it is considered to be the most evolved of the rocks examined (Table I).

Olivine is found in all the samples excepting SN15 (that in which free quartz occurs) and usually occurs either as euhedral crystals or as subhedral to anhedral inclusions in clinopyroxene. Annular zones of inclusions as reported by Naidu (1963) are rare and, when they occur, there does not appear to be any detectable optical zonation of the olivines.

Orthopyroxene is a new discovery in this sequence of rocks, occurring in several of the samples (Table I). Since there is an association with olivine, with rare overgrowths on embayed olivine (SN67), this mineral is considered to be next in terms of petrographic evolution. In many cases the orthopyroxene is associated with a symplectite or vermicular intergrowth of magnetite and minor green spinel (fig. 2*b*). Texturally it is possible that the orthopyroxene has exsolved the spinel phases during cooling, though this hypothesis may lead to an unrealistic composition for the orthopyroxene if the relative amounts of the mineral phases are considered. An alternative hypothesis is that olivine has been partially replaced by bronzite, spinel, and magnetite (cf. Ambler and Ashley, 1977; Goode, 1974).

The clinopyroxenes have previously only been studied optically; however, the compositions reported by Naidu (1963) agree well with the compositions determined in this study varying through diopside–salite–augite. The crystals are frequently euhedral and commonly show zoning which may be paralleled by annular trains of inclusions. Other crystals occur as subhedral to anhedral aggregates and show little or no optical zonation. There are no lamellar structures present other than schiller texture developed in the clinopyroxenes of some samples. The development is variable, in one case being developed in the core and surrounded with a non-schillered rim whilst in other instances schiller is only developed in the marginal zone.

Another mineral which has not previously been reported from this suite is amphibole. In the gabbroic SN15 and ultramafic SN66 green amphiboles occur whilst in the ultramafic SN106 there is a brownish variety. Texturally the relationship of the amphibole to the clinopyroxene is either one of overgrowth (fig. 2*c*) or apparent independence, occurring either as euhedral crystals or interstitially. The overgrowth in SN15 is particularly interesting as it occurs as a concentric layer within the clinopyroxene. This would suggest that the amphibole crystallized during the crystallization of the clinopyroxene. However, approximately the same composition series amphibole occurs as euhedral prisms, often showing polysynthetic or simple twinning, and apparently unrelated to any of the clinopyroxenes. It is further emphasized that the relationship is not that of a pseudomorph. The euhedral amphiboles, together with intergrown, subhedral to anhedral clinopyroxenes are poikilitically enclosed within plates of feldspar, which reinforces the textural interpretation that these minerals are related by sequential igneous crystallization. In SN66, as well as occurring as subhedral, interstitial grains the amphibole occurs both as a marginal phase and occupies other concentric zones in some clinopyroxene crystals. The textural similarity of the amphiboles in these two samples and the evidence of the sequence of inclusion would appear to conclusively rule out a later, metamorphic or deuteric alteration origin for the amphibole. The amphibole in SN106 is very different in its texture since it occurs predominantly as an intercumulus phase between the other mafic minerals, suggesting that it crystallized last of all. This type of relation clearly rules out any later origin and firmly places the amphibole as a part of the primary igneous crystallization sequence.

Phlogopite occurs sporadically in the samples examined in minor amounts (Table I). Commonly it occurs as a reaction rim around scattered magnetite grains often associated with green spinel, but it may also be found as interstitial flakes, particularly along some of the contacts between potassium feldspar and the other mafic phases. There are also sporadic phlogopite inclusions in some of the early formed clinopyroxene crystals. Apatite prisms (and rare calcite in one or two samples) complete the usual mineral assemblage with a little epidote occurring in SN15.

In all the samples studied there appears to be an overall trend of increasing silica saturation and a related sequence of inclusion of the mineral phases. The sequence of crystallization would appear to be firstly euhedral to subhedral olivine which is enclosed by the later euhedral clinopyroxene. The euhedral olivines are presumably crystals which escaped inclusion during co-precipitation with

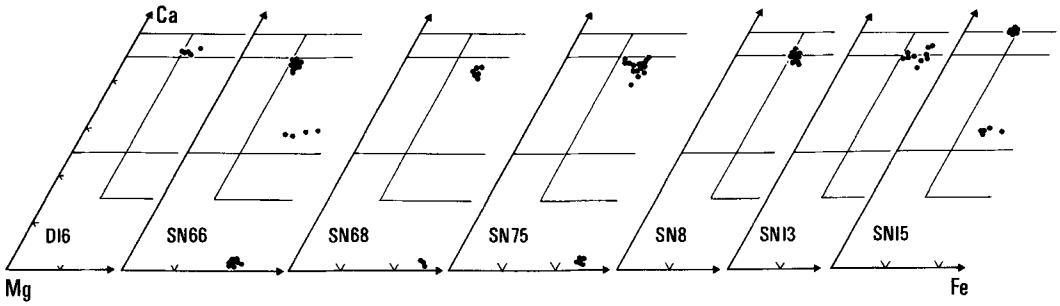

FIG. 3. The system Ca–Mg–Fe with the compositions of the analysed orthopyroxenes, clinopyroxenes. The coexisting amphiboles in samples SN66 and SN15 are also shown.

clinopyroxene. The subhedral, unzoned aggregates of clinopyroxene follow.

Orthopyroxene and the intergrown spinel phases are more difficult to place accurately. In SN75 olivine + orthopyroxene + spinel are found as inclusions inside clinopyroxene as well as occurring amongst a clinopyroxene + olivine aggregate. In the two appropriate samples amphibole closely follows and is partly synchronous with the growth of clinopyroxene. Euhedral potassium feldspar prisms and aggregates follow with poikilitic potassium feldspar and the interstitial intergrowths of nepheline and potassium feldspar later. Quartz occurs in a similar interstital position or as late intergrowths with alkali feldspar in SN15.

This type of sequence of inclusion accounts for the optical zonation and the annular arrangement of inclusions observed in the euhedral phenocryst phases and also explains the unzoned aggregates of clinopyroxene. In addition, it follows a simple evolutionary path that may be related to an increase in silica saturation and a change in water-vapour pressure conditions as crystallization proceeded.

Mineral chemistry. Using the petrographic evidence presented above, a rational sequence of crystallization may be deduced for the shonkinitic rocks. This evolution may therefore be represented in the mineral chemistry. Of the minerals present perhaps the most useful in normal circumstances for petrogenetic purposes are the clinopyroxenes (Deer *et al.*, 1978).

Representative analyses, structural formulae, and end-member compositions are presented in Table II whilst the compositions of the analysed pyroxenes are plotted in figs. 3, 4, and 5. Most of the clinopyroxenes may be adequately represented by the three end members Di–Hed–Ac. The other components being relatively small and, under the conditions postulated Na is not thought to combine with Al. In the system Ca–Fe–Mg (fig. 3) it is evident that overall the clinopyroxenes only show a limited evolutionary sequence but in any one sample there are specific relationships which may be observed. When plotted in the system Na–Mg–Fe (fig. 4) it is apparent that they are relatively unevolved when compared with clinopyroxenes from other alkaline rocks (Stephenson, 1972; Larsen, 1976; Parsons, 1979; Mitchell, 1980). However, in this system there does appear to be a rational sequence that fits the petrographic sequence of crystallization and the trend for increase in silica saturation.

In general, it can be seen (fig. 3) that the pyroxenes are relatively magnesian and that there is little iron enrichment, although this type of continuous zonation may be demonstrated in any one phenocryst, the core being more magnesian than the margins (e.g. SN75, fig. 5). Apart from the zoning towards the margins there is little difference between the composition of the clinopyroxene phenocrysts and the aggregates. Also, for the given coexisting orthopyroxene the clinopyroxene appears to be slightly more magnesian, as expected.

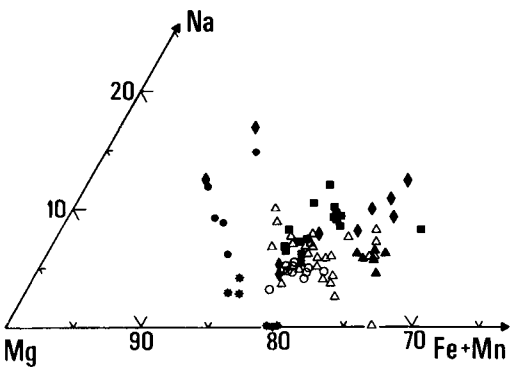

FIG. 4. Composition of the clinopyroxenes in the system Na–Mg–Fe, which is essentially equivalent to Ac–Di–Hed. Symbols: dots = D16; squares = SN8; diamonds = SN13; stars = SN15; open circles = SN66; solid triangles = SN68; open triangles = SN75.

TABLE II. Representative analyses of clinopyroxenes from the Salem shonkinitic rocks

	D16				SN66							SN68				SN75				
	01	02	04	05	2*	3*	4*	7*	1A	1B	2A	1	2	4	6	1A	1D	1G	1I	
SiO_2	50.5	51.0	52.1	51.9	52.21	52.77	51.93	51.60	51.4	52.1	53.4	51.2	50.8	51.2	50.5	51.2	52.4	52.2	50.7	SiO_2
TiO_2	0.75	0.57	0.39	0.39	0.32	0.32	0.34	0.17	0.27	0.28	0.26	0.39	0.67	0.46	0.43	0.53	0.49	0.41	0.59	TiO_2
Al_2O_3	5.34	3.64	2.95	2.75	2.96	3.13	3.16	2.00	2.79	2.81	2.81	3.94	4.52	3.91	4.11	4.14	2.67	3.36	4.30	Al_2O_3
Cr_2O_3	0.19	0.30	0.36	0.34	na	na	na	na	0.41	0.32	0.36	0.31	0.28	0.36	0.38	0.31	0.26	0.42	0.27	Cr_2O_3
V_2O_5	nd	nd	nd	nd	na	na	na	na	nd	nd	nd	0.14	nd	nd	nd	0.12	nd	nd	nd	V_2O_5
FeO	7.57	6.61	6.54	6.49	6.55	6.29	6.43	6.22	6.47	6.73	7.26	9.27	8.62	8.28	8.19	9.10	6.72	7.86	8.26	FeO
MnO	0.19	nd	0.12	nd	0.22	0.22	0.19	0.16	0.14	0.14	0.21	0.17	0.15	0.15	0.15	0.20	0.17	0.23	0.23	MnO
MgO	12.4	14.7	14.4	14.4	15.78	15.56	15.21	15.99	15.8	15.4	14.9	14.7	14.1	14.7	13.8	15.3	15.3	15.5	13.9	MgO
NiO	nd	nd	nd	nd	na	na	na	na	nd	nd	nd	nd	nd	nd	nd	nd	0.15	nd	nd	NiO
ZnO	nd	nd	nd	nd	na	na	na	na	nd	nd	nd	nd	nd	nd	0.20	nd	nd	nd	nd	ZnO
CaO	20.6	20.7	21.4	21.3	20.14	20.93	21.01	20.94	20.6	20.5	20.5	18.8	19.3	18.8	20.0	18.0	21.2	19.2	19.8	CaO
Na_2O	1.91	1.63	1.22	1.30	0.79	0.82	0.79	0.51	1.01	0.90	0.71	1.03	0.91	0.98	1.06	0.98	1.08	0.71	1.11	Na_2O
K_2O	nd	nd	nd	nd	0.03	0.03	0.03	0.03	nd	nd	nd	nd	nd	nd	nd	nd	nd	nd	nd	K_2O
Total	99.45	98.45	99.48	98.87	99.00	100.07	99.09	97.62	98.62	99.18	99.41	99.95	99.35	98.84	98.72	99.88	100.44	99.89	99.16	Total
Cations on the basis of 6(O)																				
Si	1.886	1.912	1.934	1.939	1.938	1.937	1.930	1.946	1.918	1.935	1.946	1.904	1.895	1.914	1.900	1.898	1.929	1.926	1.898	Si
Al^{iv}	0.114	0.088	0.066	0.061	0.062	0.063	0.070	0.054	0.082	0.065	0.054	0.096	0.105	0.086	0.100	0.102	0.071	0.074	0.102	Al^{iv}
Al^{vi}	0.121	0.073	0.063	0.060	0.067	0.068	0.068	0.034	0.041	0.058	0.069	0.076	0.094	0.086	0.082	0.079	0.045	0.072	0.087	Al^{vi}
Ti	0.021	0.016	0.011	0.011	0.009	0.009	0.009	0.005	0.007	0.008	0.007	0.011	0.019	0.013	0.012	0.015	0.013	0.011	0.017	Ti
Cr	0.006	0.009	0.011	0.010	-	-	-	-	0.012	0.010	0.010	0.009	0.008	0.011	0.011	0.009	0.008	0.012	0.008	Cr
V	-	-	-	-	-	-	-	-	-	-	-	0.004	-	-	-	0.004	-	-	-	V
Fe	0.236	0.207	0.203	0.203	0.203	0.193	0.200	0.196	0.202	0.209	0.226	0.288	0.269	0.259	0.258	0.282	0.207	0.243	0.259	Fe
Mn	0.006	-	0.004	-	0.007	0.007	0.006	0.005	0.005	0.004	0.007	0.005	0.005	0.005	0.005	0.006	0.005	0.007	0.007	Mn
Mg	0.692	0.789	0.797	0.803	0.873	0.852	0.843	0.899	0.881	0.854	0.822	0.814	0.782	0.819	0.774	0.844	0.841	0.851	0.774	Mg
Ni	-	-	-	-	-	-	-	-	-	-	-	-	-	-	-	-	0.004	-	-	Ni
Zn	-	-	-	-	-	-	-	-	-	-	-	-	-	-	0.005	-	-	-	-	Zn
Ca	0.822	0.833	0.852	0.852	0.800	0.823	0.843	0.846	0.823	0.816	0.814	0.748	0.774	0.753	0.774	0.716	0.835	0.760	0.794	Ca
Na	0.138	0.119	0.088	0.094	0.057	0.058	0.057	0.038	0.073	0.065	0.051	0.074	0.066	0.071	0.077	0.070	0.077	0.051	0.080	Na
K	-	-	-	-	0.001	0.002	0.002	0.002	-	-	-	-	-	-	-	-	-	-	-	K

	SN 75				SN8					SN13				SN15						
	1M	2A	5	7B	1A	1G	2B	3D	3E	2A	2C	2E	3	1	2	3	5	8	9	
SiO_2	52.2	50.9	50.1	51.6	51.3	51.9	52.2	51.0	51.8	50.3	53.2	51.2	50.4	54.5	54.2	54.9	54.7	53.9	54.4	SiO_2
TiO_2	0.42	0.36	0.44	0.38	0.50	0.43	0.30	0.59	0.51	0.84	0.21	0.59	0.83	nd	nd	nd	nd	nd	nd	TiO_2
Al_2O_3	3.06	3.95	3.93	2.53	3.77	2.81	2.95	4.65	3.80	6.36	3.73	4.25	6.23	0.27	0.36	nd	0.23	0.22	0.30	Al_2O_3
Cr_2O_3	0.24	0.46	0.37	0.56	0.29	0.22	0.35	0.32	0.29	0.19	0.40	0.31	0.21	0.23	0.26	0.30	0.25	0.24	0.26	Cr_2O_3
V_2O_5	0.12	nd	nd	nd	nd	nd	nd	nd	nd	nd	nd	nd	0.15	nd	nd	nd	nd	nd	nd	V_2O_5
FeO	7.37	9.12	8.83	7.39	7.05	6.66	6.47	6.53	6.97	7.85	6.80	8.11	7.70	5.59	5.95	5.72	5.62	5.39	5.76	FeO
MnO	0.15	0.23	0.24	0.14	nd	0.20	nd	nd	0.17	nd	nd	0.14	0.12	0.12	0.15	nd	nd	0.14	0.16	MnO
MgO	14.9	15.1	14.5	14.7	14.5	14.9	15.1	13.8	14.3	11.9	14.2	13.3	12.0	14.1	14.2	14.4	14.4	14.1	13.9	MgO
NiO	nd	nd	nd	nd	nd	nd	nd	nd	nd	nd	0.15	nd	nd	nd	nd	nd	nd	nd	nd	NiO
ZnO	nd	nd	0.21	nd	nd	nd	nd	nd	nd	nd	nd	nd	nd	nd	nd	nd	nd	nd	nd	ZnO
CaO	20.5	18.2	18.6	20.4	19.9	20.8	20.6	20.4	19.9	20.2	20.5	19.8	20.3	24.3	24.1	24.5	24.4	24.3	24.6	CaO
Na_2O	0.90	0.59	0.86	0.50	1.60	1.09	1.68	1.83	1.43	2.13	1.75	1.67	1.80	nd	0.58	nd	0.38	0.44	nd	Na_2O
K_2O	nd	nd	nd	nd	nd	nd	nd	nd	nd	nd	nd	nd	nd	nd	nd	nd	nd	nd	nd	K_2O
Total	99.86	98.91	98.08	98.20	98.91	99.01	99.65	99.12	98.37	99.77	98.24	99.37	99.74	99.11	100.50	100.01	100.22	98.73	99.38	
Cations on the basis of 6(O)																				
Si	1.930	1.905	1.900	1.942	1.915	1.934	1.932	1.898	1.913	1.870	1.942	1.911	1.873	2.024	2.007	2.023	2.015	2.013	2.019	Si
Al^{iv}	0.070	0.095	0.100	0.058	0.085	0.066	0.068	0.102	0.087	0.130	0.058	0.089	0.127	-	-	-	-	-	-	Al^{iv}
Al^{vi}	0.064	0.079	0.075	0.054	0.081	0.057	0.061	0.102	0.081	0.149	0.103	0.099	0.146	0.012	0.016	-	0.010	0.010	0.013	Al^{vi}
Ti	0.012	0.010	0.013	0.011	0.014	0.012	0.008	0.017	0.014	0.023	0.006	0.016	0.023	-	-	-	-	-	-	Ti
Cr	0.007	0.014	0.011	0.017	0.009	0.006	0.010	0.009	0.009	0.006	0.012	0.009	0.006	0.007	0.009	0.009	0.007	0.007	0.008	Cr
V	0.004	-	-	-	-	-	-	-	-	-	-	-	0.005	-	-	-	-	-	-	V
Fe	0.228	0.285	0.280	0.233	0.220	0.208	0.200	0.203	0.219	0.244	0.208	0.253	0.239	0.174	0.184	0.176	0.173	0.168	0.179	Fe
Mn	0.005	0.007	0.008	0.004	-	0.006	-	-	0.006	-	-	0.005	0.004	0.004	0.005	-	0.007	0.004	0.005	Mn
Mg	0.824	0.844	0.817	0.824	0.809	0.827	0.834	0.767	0.802	0.660	0.772	0.742	0.665	0.781	0.784	0.790	0.788	0.786	0.767	Mg
Ni	-	-	-	-	-	-	-	-	-	-	-	-	-	-	-	-	-	-	-	Ni
Zn	-	-	0.006	-	-	-	-	-	-	-	-	-	-	-	-	-	-	-	-	Zn
Ca	0.812	0.730	0.753	0.823	0.794	0.833	0.817	0.815	0.800	0.806	0.801	0.792	0.808	0.967	0.975	0.966	0.963	0.974	0.980	Ca
Na	0.064	0.043	0.063	0.037	0.116	0.079	0.121	0.132	0.104	0.154	0.124	0.121	0.130	-	0.042	-	0.027	0.032	-	Na
K	-	-	-	-	-	-	-	-	-	-	-	-	-	-	-	-	-	-	-	K

na: not analysed; nd: not detected; * SN66 WDS analyses, all others EDS analyses.

In fig. 4 one of the most undersaturated rocks (D16) has overall the most sodic clinopyroxenes. However, in the evolutionary sequence of some pyroxenes in SN13, the compositions of the rims may exceed those values. It is also evident that, generally with increasing silica saturation, the analyses plot progressively towards more magnesium-poor compositions. The zonation which occurs is interesting because it sometimes goes against the overall sequence, the pyroxenes in SN13, for example, having less sodic, more iron-rich cores zoned to more sodic, more magnesian rims. Complex zonation of pyroxenes, repeating or reversing the overall trend such as this, has been reported in alkaline rocks (e.g. Mitchell, 1980).

Throughout the clinopyroxenes there is a rational relationship between Al, Ti, and Na with Si. Using the SiO_2 *vs.* Al_2O_3 index of Le Bas (1962) the clinopyroxenes overlap the boundary between the non-alkaline and alkaline fields. All of the analyses

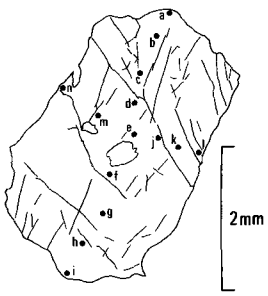

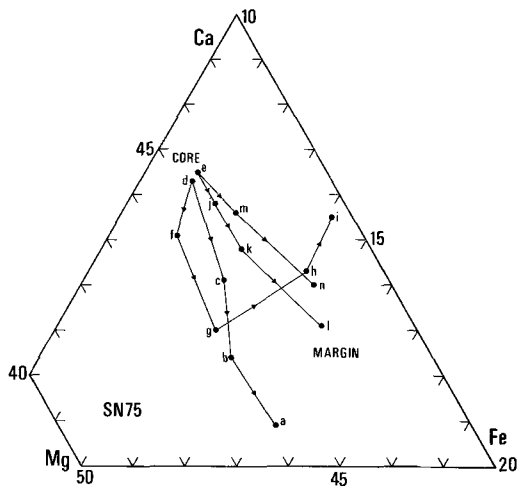

FIG. 5. Composition of one clinopyroxene phenocryst (grain 1) from SN75 showing the zonation from a magnesian core to a more iron-rich margin. The variation in the Ca content is considered to be due to the adjoining phases.

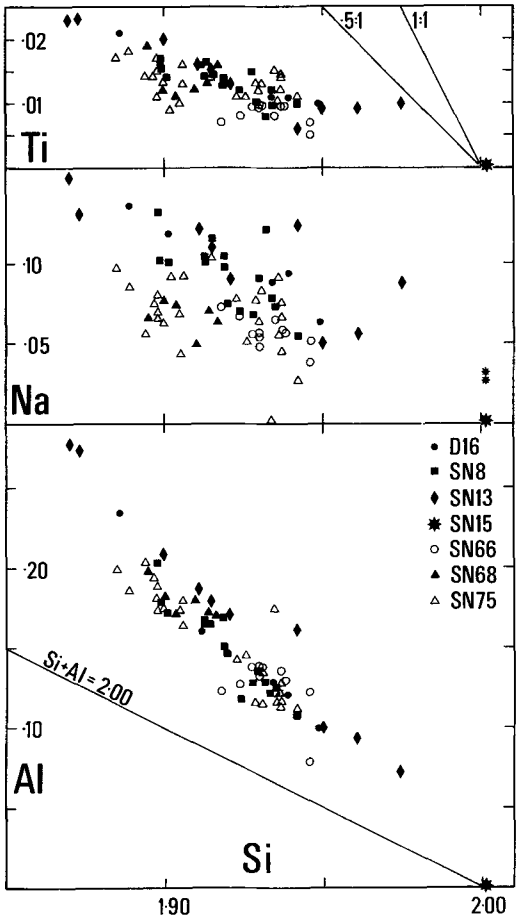

FIG. 6. Variation of the clinopyroxenes in terms of Si versus Al, Ti, and Na.

lie on the Al side of the Si + Al = 2.00 reference line (fig. 6). Gibb (1973) has suggested that in cases of sympathetic Si–Ti variation, such as this, the substitution operating is $M + 2Si \rightleftharpoons Ti + 2Al$. This requires that the Al : Si and Ti : Si slopes should be 1 : 1 and 0.5 : 1 respectively, which is not the case here (fig. 6). To allow for such a circumstance Gibb (1973) suggests a further substitution, $M + Si \rightleftharpoons Al + Al$, which, since the slope of the Ti : Si slope is less than 0.5 : 1 could be operating. A corresponding increase in Na is seen with increasing Al with decreasing Si. Whilst this supports a relationship between the rocks there is conflicting evidence as to the direction of fractionation trends; for example, Al increases (Smith and Carmichael, 1969) or decreases (Smith and Lindsley, 1971). It is clear that there is sufficient Al after balancing the Si deficiency to balance the Na present, probably according to

TABLE III. Representative analyses of orthopyroxenes from the Salem shonkinitic rocks

	SN66*				SN68			SN75						
	a	2	4	8	1	2	3	1A	1B	2A	3B	12	15	
SiO_2	54.22	54.18	54.95	54.45	53.0	52.8	53.0	53.4	53.3	53.8	53.8	53.1	53.0	SiO_2
TiO_2	0.11	0.18	0.05	0.15	nd"	0.12	0.15	0.14	0.12	nd	0.15	nd	nd	TiO_2
Al_2O_3	2.04	2.11	1.03	2.12	2.58	2.36	2.65	3.69	3.29	2.42	2.10	2.36	2.43	Al_2O_3
Cr_2O_3	na'	na	na	na	0.13	0.14	0.12	nd	0.12	0.17	nd	0.16	0.17	Cr_2O_3
FeO	13.00	12.89	10.02	13.36	15.6	16.0	15.6	15.7	15.3	15.5	15.1	15.6	15.7	FeO
MnO	0.35	0.33	0.28	0.34	0.22	0.30	0.34	0.32	0.28	0.32	0.25	0.27	0.27	MnO
MgO	28.49	28.54	28.79	28.75	26.7	26.8	27.0	26.4	26.3	26.9	27.1	26.8	26.9	MgO
NiO	na	na	na	na	nd	nd	nd	nd	nd	nd	nd	nd	nd	NiO
CaO	0.86	1.07	0.69	0.94	0.99	0.62	1.01	1.05	0.79	1.10	1.01	0.99	1.03	CaO
Na_2O	0.06	0.03	0.03	0.03	nd	nd	nd	nd	nd	nd	nd	nd	nd	Na_2O
K_2O	0.04	0.04	0.04	0.04	nd	nd	nd	nd	nd	nd	nd	nd	nd	K_2O
Total	99.17	99.37	99.79	100.18	99.22	99.14	97.87	100.70	99.50	100.17	99.51	99.28	99.60	
Cations on the basis of 6(O)														
Si	1.950	1.945	1.959	1.942	1.931	1.927	1.919	1.908	1.929	1.940	1.947	1.934	1.926	Si
Al^{iv}	0.050	0.055	0.041	0.058	0.069	0.073	0.081	0.092	0.071	0.060	0.053	0.066	0.074	Al^{iv}
Al^{vi}	0.036	0.034	0.041	0.031	0.042	0.028	0.032	0.063	0.070	0.043	0.046	0.035	0.030	Al^{vi}
Ti	0.003	0.005	0.002	0.004	-	0.003	0.004	0.004	0.003	-	0.004	-	-	Ti
Cr	-	-	-	-	0.004	0.004	0.004	-	0.004	0.005	-	0.005	0.005	Cr
Fe	0.391	0.387	0.385	0.398	0.475	0.488	0.472	0.469	0.463	0.466	0.456	0.475	0.478	Fe
Mn	0.011	0.010	0.011	0.010	0.007	0.009	0.010	0.010	0.009	0.008	0.008	0.008	0.008	Mn
Mg	1.528	1.527	1.531	1.529	1.447	1.460	1.457	1.407	1.417	1.442	1.462	1.451	1.458	Mg
Ni	-	-	-	-	-	-	-	-	-	-	-	-	-	Ni
Ca	0.033	0.041	0.026	0.036	0.039	0.024	0.039	0.040	0.030	0.043	0.039	0.039	0.040	Ca
Na	0.005	0.002	0.002	0.002	-	-	-	-	-	-	-	-	-	Na
K	0.002	0.002	0.002	0.002	-	-	-	-	-	-	-	-	-	K

"nd: not detected; 'na: not analysed; *SN66 by WDS analysis, all others by EDS.

$Na + Al \rightleftharpoons Ca + M$ (cf. Gibb, 1973). SN15 has the least sodic pyroxenes—diopsides—and has a sodium-poor amphibole as part of its mafic sequence of crystallization. However, it is considered to be late, since it contains free quartz. The sodium-bearing phase is now albitic plagioclase instead of the mafic phases which are now sodium-poor (Tables I, II, and V).

Orthopyroxene coexisting with clinopyroxene has been analysed in three of the samples (Table III). In each case the orthopyroxene is a bronzite, with that occurring in the more ultramafic example being slightly more magnesian than those occurring in the gabbroic samples (fig. 3). The coexisting pairs of pyroxenes have been utilized for geothermometry (Table IV). The bronzites are commonly associated with magnetite and green hercynite. The origin of this intergrowth is not clear since similar composition magnetite-hercynite intergrowths are found without bronzite but mantled with phlogopite. Goode (1974) suggested that such a symplectite could result from the sub-solidus oxidation of olivine in the compositional range Fo_{63}–Fo_{75}. Whilst this partly covers

TABLE IV. Geothermometry of co-existing phases

	1	2	3
D16	-	-	1037 1039
SN8	-	-	1046 1048
SN13	-	-	1053 1067
SN66	977 1014	953 1002	1037 1061
SN68	931 1003	939 1023	1041 1058
SN75	921 1041	996 1070	1042 1074

1. Wells (1977) opx-cpx
2. Wood and Banno (1973) opx-cpx
3. Powell and Powell (1974) ol-cpx.

An arbitrary value of 5kbar has been assumed for the determination of the Powell and Powell (1974) olivine-clinopyroxene geothermometer. For a value of 1kbar the temperatures calculated are approximately 20°C lower, so the temperatures calculated are possible maxima.

TABLE V. Representative analyses of olivines in the Salem shonkinitic rocks

	D16					SN66					SN68			
	I1	I2	1	3	4	1	2	3	4*	5*	o1	o2	o3	
SiO_2	40.2	40.0	38.7	38.7	39.2	39.3	39.3	39.7	39.14	38.99	38.2	38.0	37.9	SiO_2
FeO	10.0	9.5	23.1	21.2	21.0	19.9	20.1	19.0	20.02	21.06	25.7	25.5	25.0	FeO
MnO	nd	0.11	0.36	0.22	0.38	0.23	0.22	0.20	0.32	0.35	0.30	0.21	0.27	MnO
MgO	50.4	49.4	38.2	40.7	40.6	40.6	40.9	41.8	41.06	40.29	37.2	37.0	37.4	MgO
NiO	0.28	0.25	0.20	0.20	nd'	0.16	0.22	0.16	na"	na	nd	nd	nd	NiO
CaO	nd	nd	0.11	0.13	nd	0.15	0.17	0.08	0.01	0.01	0.13	nd	nd	CaO
Total	100.88	99.26	100.67	101.15	101.18	100.34	100.91	100.94	100.55	100.70	101.53	100.71	100.57	
Cations on the basis of 4(O)														
Si	0.992	0.989	1.004	0.989	1.000	1.006	1.003	1.005	1.000	1.000	0.995	0.996	0.993	Si
Fe	0.201	0.196	0.501	0.454	0.448	0.426	0.428	0.403	0.428	0.452	0.559	0.559	0.547	Fe
Mn	-	0.002	0.008	0.005	0.008	0.005	0.005	0.004	0.006	0.008	0.007	0.005	0.006	Mn
Mg	1.809	1.818	1.476	1.551	1.544	1.550	1.553	1.578	1.564	1.540	1.441	1.444	1.460	Mg
Ni	0.005	0.005	0.004	0.004	-	0.003	0.004	0.003	-	-	-	-	-	Ni
Ca	-	-	0.003	0.004	-	0.004	0.005	0.002	-	-	0.004	-	-	Ca
Fo	90.0	90.2	74.7	77.4	77.5	78.5	78.4	79.7	78.5	77.3	72.1	72.1	78.2	Fo

'nd: not detected; "na: not analysed; * WDS analyses, others EDS analyses.

	SN75					SN8					SN13			
	1A	1	2	1R	14	1	2	3	7	8	1A	1B	5B	8A
SiO_2	37.8	39.2	38.9	38.9	38.0	40.1	39.6	39.8	39.8	39.2	37.7	38.0	38.6	38.5
FeO	23.7	21.3	24.8	24.0	24.9	17.5	17.8	17.6	16.7	16.5	25.6	25.2	24.0	25.4
MnO	0.31	0.29	0.21	0.32	0.32	0.28	0.26	0.32	0.24	0.27	0.33	0.36	0.35	0.40
MgO	36.4	40.2	37.2	38.5	37.1	42.8	42.3	42.7	43.4	43.3	35.9	35.6	36.7	35.9
NiO	nd	0.16	nd	nd	nd	0.16	nd	0.21	0.16	0.21	nd	nd	nd	0.16
CaO	0.10	0.15	0.11	nd	nd	0.21	0.18	0.20	0.15	0.15	0.12	0.12	0.16	0.10
Total	98.31	101.30	101.22	101.72	100.32	101.05	100.14	100.83	100.45	99.63	99.65	99.32	99.81	100.46
Cations on the basis of 4(O)														
Si	1.007	0.998	1.009	1.000	0.997	1.005	1.006	1.003	1.000	0.993	1.001	1.010	1.012	1.010
Fe	0.528	0.453	0.538	0.516	0.546	0.367	0.377	0.371	0.352	0.350	0.568	0.560	0.547	0.559
Mn	0.007	0.006	0.005	0.003	0.007	0.006	0.007	0.007	0.005	0.006	0.008	0.008	0.008	0.009
Mg	1.477	1.523	1.436	1.474	1.452	1.596	1.600	1.605	1.624	1.633	1.419	1.409	1.436	1.406
Ni	-	0.003	-	-	-	0.003	-	0.004	0.003	0.004	-	-	-	0.003
Ca	0.003	0.004	0.003	-	-	0.006	0.005	0.005	0.004	0.004	0.004	0.004	0.004	0.003
Fo	73.2	77.1	72.8	74.1	72.7	81.3	80.9	81.2	82.2	82.3	71.4	71.6	73.1	71.6

nd: not detected.

the compositional range of the olivines present (Table V) there is no evidence of there having been a more iron-rich phase. Also, the bronzites fall in a part of the normal trend for igneous crystallization (Deer *et al.*, 1978). Goode (1974) further suggests that for olivines of composition Fo_{75}–Fo_{84} a spinel-orthopyroxene intergrowth would develop upon decomposition. Whilst green hercynite is associated with magnetite and bronzite it is not in a symplectic relationship and therefore this origin is discounted.

The olivines are of two distinct varieties (Table V). First, there is the common euhedral to subhedral grains which are of consistant composition between Fo_{70}–Fo_{80}. These olivines are considered to be the products of the crystallization sequence. In addition in D16, there are one or two rare examples of olivines with a composition of Fo_{90}. These are only found as embayed inclusions within clinopyroxene and are otherwise not optically distinguishable. They are considered to be xenocrysts derived from the dunite, which is a probable

TABLE VI. Microprobe analyses of the amphiboles

	SN66				SN15					
	1A	1B	1C	1D	1	2	3	4	5	
SiO_2	42.7	44.1	44.1	42.7	54.2	55.8	54.4	55.6	51.3	SiO_2
TiO_2	1.46	0.94	1.23	1.63	nd	nd	nd	nd	0.35	TiO_2
Al_2O_3	12.4	11.4	11.8	12.1	2.77	1.51	2.39	1.75	5.88	Al_2O_3
Cr_2O_3	0.37	0.48	0.31	0.41	0.22	0.22	0.23	0.25	0.14	Cr_2O_3
FeO*	9.10	11.3	8.15	9.58	8.73	8.19	7.84	7.89	9.67	FeO
MnO	nd	nd	nd	nd	0.11	0.16	0.24	0.19	0.18	MnO
MgO	15.7	13.9	16.3	14.8	17.6	18.8	18.3	18.5	16.3	MgO
CaO	11.6	11.9	11.7	11.7	12.9	12.9	12.8	12.9	12.2	CaO
Na_2O	2.92	2.46	2.68	2.50	nd	0.44	nd	0.66	1.31	Na_2O
K_2O	0.54	nd	0.13	1.02	0.19	0.07	0.13	nd	0.37	K_2O
Total	96.79	96.48	96.30	96.44	96.72	98.07	96.33	97.74	97.70	
Cations on the basis of 23(O)										
Si	6.273	6.513	6.432	6.316	7.740	7.837	7.768	7.828	7.336	Si
Al	1.727	1.487	1.568	1.684	0.260	0.163	0.232	0.172	0.664	Al
Al	0.423	0.505	0.456	0.430	0.206	0.087	0.170	0.118	0.327	Al
Cr	0.042	0.056	0.035	0.048	0.025	0.024	0.026	0.028	0.015	Cr
Ti	0.161	0.105	0.134	0.182	-	-	-	-	0.037	Ti
Mg	3.429	3.059	3.554	3.263	3.737	3.932	3.893	3.878	3.477	Mg
Fe^{2+}	0.945	1.275	0.821	1.077	1.032	0.957	0.911	0.939	1.144	Fe^{2+}
Mn	-	-	-	-	-	-	-	0.022	-	Mn
Fe^{2+}	0.172	0.115	0.176	0.108	0.010	0.007	0.026	-	0.013	Fe^{2+}
Mn	-	-	-	-	0.013	0.019	0.028	-	0.022	Mn
Ca	1.828	1.885	1.824	1.858	1.974	1.937	1.946	1.939	1.872	Ca
Na	-	-	-	0.034	-	0.037	-	0.061	0.093	Na
Ca	0.004	0.006	0.005	-	-	-	0.006	-	-	Ca
Na	0.831	0.703	0.759	0.683	-	0.083	-	0.188	0.271	Na
K	0.101	-	0.023	0.192	0.034	0.012	0.024	-	0.067	K
Mg/(Mg+Fe)	75.4	68.8	78.1	73.4	78.2	80.3	80.5	80.6	75.0	

* All Fe determined as FeO. The structural formulae were calculated according to Leake (1978).

nd = not detected.

origin particularly since dunite xenoliths occur in the shonkinite.

The amphiboles (Table VI) vary in composition from actinolite through actinolitic hornblende to tschermakitic hornblende using the nomenclature of Leake (1978). Plotted with their coexisting pyroxenes (fig. 3) they rationally fit a sequence of progressive crystallization being slightly more iron-rich but are still relatively magnesian (Mg/(Mg+Fe) 75–80, Table VI). If they had formed by some other process, such as the replacement of clinopyroxene, it is unlikely that they would plot in this manner and would also involve the mobility of components for which there is no evidence. The modification associated with the magnesite formation causes severe alteration of the mafic phases (particularly olivine) which does not occur in the analysed samples.

The fingerprint textures in the three rocks in which they occur (D16, SN101, SN103) are so fine that they cannot be resolved optically or under the probe beam (fig. 2*a*). However, it is evident that they consist of two distinct phases, although the analyses clearly represent mixtures (Table VII). The intergrowths consist of a silica-poor, sodium-rich phase and a silica-rich, potassium-rich, sodium-poor phase. The interpretation that best fits this is an intergrowth of nepheline and potassium feldspar. Such composition fingerprint textures have previously been reported in other alkaline rocks (Davidson, 1970; Mitchell and Platt, 1980), whilst nepheline–potassium–feldspar solid solutions are a common occurrence in undersaturated basic rocks (Tilley, 1954; Tuttle and Smith, 1958; Deer *et al.*, 1963). Naidu (1963) also described symplectites of nepheline and sanidine though no intergrowths as coarse as those figured have been found in this study.

The feldspars occurring in the other samples, with the exception of SN15, all contain a mixture of potassium and sodium feldspar (Table VII, fig. 7), sanidines (cf. Naidu, 1963). The analyses of the

intergrowths are also plotted in fig. 7 for comparison and they are clearly much more sodic, as well as being too low in silica (Table VII). The feldspars may be divided into textural types as described earlier, which are also distinct chemically and fall into three groups: (i) non-perthitic, uniform potassium feldspar which comprises both that intergrown with quartz and interstitial material—this is generally less sodic (*c.* 10% albite) than similar feldspar in other samples; (ii) perthitic potassium feldspar containing albitic blebs—these albitic areas are slightly potassic (fig. 7); (iii) albitic plagioclase containing little or no potassium feldspar (fig. 7) but with antiperthites of low sodium content.

TABLE VII. Analyses of the nepheline - K-feldspar fingerprint intergrowths and representative analyses of feldspars for comparison

	D16									SN68				
	intergrowths							sanidines						
	I1	I2	I3	I4	I5	I6	I7	1	2	1	2	4	5	
SiO_2	55.2	61.7	56.8	57.9	59.8	58.7	59.0	63.0	64.0	62.8	63.3	65.0	62.9	SiO_2
Al_2O_3	26.0	19.7	25.2	24.3	21.8	23.3	22.2	18.8	18.7	18.9	18.3	18.9	18.9	Al_2O_3
TiO_2	nd	nd	nd	nd	nd	nd	nd	0.26	0.37	0.37	nd	nd	0.39	TiO_2
FeO	0.16	nd	0.13	0.15	0.17	0.11	0.11	nd	0.14	nd	0.17	0.18	0.18	FeO
MgO	0.23	nd	nd	nd	nd	nd	nd	nd	nd	nd	nd	0.21	nd	MgO
CaO	0.38	0.26	0.46	0.39	0.23	0.35	0.31	0.17	0.16	0.45	0.09	0.13	0.33	CaO
Na_2O	7.86	2.69	7.85	6.93	4.76	6.30	5.37	1.51	1.91	1.90	0.98	1.15	1.95	Na_2O
K_2O	10.5	13.3	11.0	11.2	12.9	11.6	12.7	13.3	13.5	12.8	14.6	14.7	12.8	K_2O
Total	100.33	97.65	101.44	100.87	99.66	100.36	99.69	96.78	98.68	97.23	97.64	100.37	97.45	
Cations on the basis of 32(O)														
Si	10.292	11.641	10.482	10.698	11.167	10.887	11.040	11.881	11.881	11.816	11.948	11.920	11.816	Si
Al	5.723	4.379	5.485	5.295	4.794	5.093	4.903	4.173	4.098	4.193	4.077	4.082	4.185	Al
Ti	-	-	-	-	-	-	-	0.037	0.051	0.052	-	-	0.055	Ti
Fe	0.025	-	0.021	0.024	0.027	0.017	0.018	-	0.021	-	0.027	0.027	0.028	Fe
Mg	0.063	-	-	-	-	-	-	-	-	-	-	-	-	Mg
Ca	0.077	0.052	0.090	0.078	0.047	0.069	0.062	0.034	0.033	0.090	0.018	0.026	0.066	Ca
Na	2.841	0.983	2.806	2.582	1.720	2.267	1.948	0.551	0.687	0.691	0.980	0.409	0.712	Na
K	2.490	3.213	2.591	2.639	3.081	2.734	3.023	3.191	3.185	3.076	3.527	3.44o	3.062	K

	SN75			SN15								
	sanidines						albites					
	1	3	5	1	2	5	11	4	6	7	9	
SiO_2	63.0	64.0	63.7	63.9	64.0	63.9	63.5	68.1	67.3	67.9	68.1	SiO_2
Al_2O_3	18.7	19.0	19.0	18.7	18.4	18.0	18.2	19.5	19.2	19.4	19.5	Al_2O_3
TiO_2	0.48	0.35	0.43	1.28	0.56	0.55	0.53	nd	nd	nd	nd	TiO_2
FeO	nd	0.15	nd	nd	nd	nd	nd	0.14	nd	nd	nd	FeO
MgO	nd	nd	nd	nd	nd	nd	nd	nd	nd	nd	nd	MgO
CaO	0.25	0.29	0.41	0.13	0.08	0.09	nd	0.61	0.35	0.41	0.32	CaO
Na_2O	1.68	1.85	1.76	0.35	0.68	0.51	0.52	11.5	11.7	11.5	11.8	Na_2O
K_2O	12.8	12.7	12.8	14.5	14.4	15.2	14.9	0.02	nd	0.09	nd	K_2O
Total	96.91	98.34	98.10	98.86	98.12	98.25	97.65	99.87	98.55	99.30	99.72	
Cations on the basis of 32(O)												
Si	11.871	11.882	11.858	11.759	11.951	11.973	11.950	11.930	11.953	11.950	11.945	Si
Al	4.151	4.151	4.164	4.179	4.059	3.982	4.145	4.032	4.014	4.029	4.028	Al
Ti	0.068	0.049	0.060	0.182	0.079	0.077	0.075	-	-	-	-	Ti
Fe	-	0.024	-	-	-	-	-	0.021	-	-	-	Fe
Mg	-	-	-	-	-	-	-	-	-	-	-	Mg
Ca	0.050	0.057	0.083	0.027	0.017	0.018	-	0.117	0.066	0.077	0.060	Ca
Na	0.615	0.665	0.637	0.127	0.248	0.186	0.188	3.892	4.011	3.938	4.015	Na
K	3.075	2.997	3.033	3.518	3.422	3.631	3.577	0.015	-	0.020	-	K

nd: not detected.

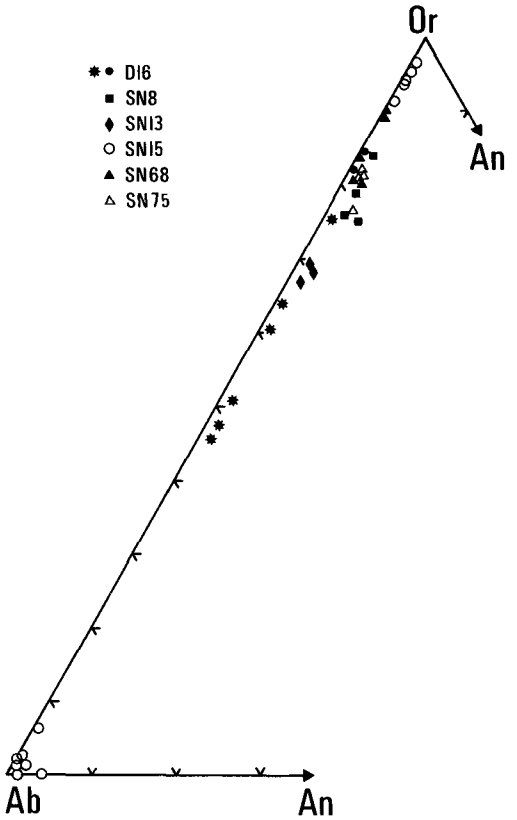

FIG. 7. Composition of the felsic phases in the system Ab–An–Or. The intergrowth structures occurring in D16 (stars) are plotted for comparison. They are clearly distinct plotting as mixtures and on inspection of Table VI are further separated by their low silica contents.

Discussion. The petrographical and mineralogical data support the progressive crystallization of a relatively magnesian, alkaline magma to form a variety of ultramafic to gabbroic-textured rocks of broadly shonkinitic composition.

Crystallization clearly begins with olivine and clinopyroxene which, under some circumstances, may give cumulates, with associated intercumulus amphibole and minor K-feldspar (Table I). The liquid then approaches the system SiO_2–$KAlSiO_3$–$NaAlSiO_4$–H_2O (Fudali, 1963; Hamilton and Mackenzie, 1965). Davidson (1970), discussing the work of Fudali (1963), proposed four possible crystallization paths to explain fingerprint textures between nepheline and K-feldspar in rocks from Kaminak Lake. He favoured a path beginning in the nepheline s.s. field, culminating in cotectic crystallization. In the Salem shonkinites the fingerprint textures occupy interstitial areas between K-feldspar, clinopyroxene, and olivine cumulus phases. Therefore, they are late, crystallizing after K-feldspar. So, whilst a cotectic origin for these intergrowths is appealing, the liquid must have entered the system in the K-feldspar field before progressing to the cotectic. This interpretation is consistent with the experimental data of Hamilton and Mackenzie (1965). However, it is very important whereabouts the liquid enters the K-feldspar field as this will dictate the phases that could potentially crystallize. This may be used to explain the interstitial nature of the feldspathoids and the association of the variety of felsic phases from leucite and pseudoleucite (Naidu, 1963) through nepheline–K-feldspar intergrowths (Naidu, 1963, and this work) to K-feldspar, Na-feldspar, and quartz, reported here for the first time.

The system $CaMgSi_2O_6$–$NaAlSiO_4$–SiO_2. (Schairer and Yoder, 1960) may be used as an analogue to describe the early mafic crystallization. In this system crystallization, which begins in the primary phase volume of forsterite, could progress to cotectic crystallization with diopside and then the cotectic crystallization of diopside + nepheline. Plagioclase appears at about 1118 °C and the system eventually crystallizes quartz at 1073 °C. In this system silica is progressively enriched in the liquid and both olivine and nepheline would be resorbed. This type of relationship is seen in some samples of the beginning of embayment of olivine and the formation of orthopyroxene. Olivine has completely disappeared from the system by the time free quartz is crystallizing (SN15). Adding iron and potassium to the system would lower the temperatues and thus the estimates obtained from the geothermometry (Table IV) appear, therefore, to be reasonable approximations.

The amphibole-bearing samples also give some indications as to the change of water-vapour pressure during crystallization, although there are no experimental data available for comparison. The formation of amphibole zones in some of the clinopyroxenes would suggest that towards the end of clinopyroxene crystallization water-vapour pressure rose causing amphibole to crystallize. However, upon the crystallization of amphibole P_{H_2O} fluctuated downwards in some samples to allow later clinopyroxene to crystallize, although evidence is not substantial enough to go any further.

This condition is, however, consistent with some of the data of Naidu (1963) who suggested that water-vapour pressure was relatively high thus reducing the field of crystallization of leucite. Pressure conditions are difficult to estimate, though there is no evidence to suggest that a separate gas phase evolved, structure such as druses

being absent. Diopsides which are rich in Tschermacks molecule are considered to have crystallized at high temperatures and pressures (Irving, 1974). Since the diopsides present here have very low tetrahedral Al, plotting at Si = 2 and have low octahedral Al (Table II), it is therefore suggested that they crystallized at relatively low pressures. This form of argument would also agree with the inference of low-pressure crystallization from the presence of sanidine in these rocks.

Acknowledgements. C.R.L.F. gratefully acknowledges financial support from the British Council in the form of ALIS awards, enabling field-work to be carried out whilst on a visit to the University of Mysore. We thank the staff of the Dalmia Magnesite Corporation for their assistance with access and discussions of their geological data. Drs. J. V. P. Long and P. Treloar are thanked for their assistance in obtaining the EDS analyses at the Department of Earth Sciences, Cambridge, and Dr N. R. Charnley for the WDS analyses at the Department of Geology, Oxford. D. J. Allen and C. G. Jones are thanked for technical assistance.

REFERENCES

Ambler, E. P., and Ashley, P. M. (1977) *Lithos*, **10**, 163–72.
Davidson, A. (1970) *Can. Mineral.* **10**, 191–206.
Deer, W. A., Howie, R. A., and Zussman, J. (1963) *Rock-forming Minerals*, **4**, Longmans, London, 435 pp.
———————(1978) Ibid. **2a**, 668 pp.
Drury, S. A., and Holt, R. W. (1980) *Tectonophys.* **65**, T1–T15.
Fudali, R. F. (1963) *Bull. geol. Soc. Am.* **74**, 1101–25.
Gibb, F. G. F. (1973) *J. Petrol.* **14**, 203–30.
Goode, A. D. T. (1974) *Nature*, **248**, 500–1.
Hamilton, D. L., and Mackenzie, W. S. (1965) *Mineral. Mag.* **34**, 214–31.
Hurlbut, C. S., and Griggs, D. (1939) *Bull. geol. Soc. Am.* **50**, 1043–112.
Irving, A. J. (1974) Ibid. **85**, 1503–14.
Larsen, L. M. (1976) *J. Petrol.* **17**, 258–90.
Le Bas, M. J. (1962) *Am. J. Sci.* **260**, 267–88.
Leake, B. E. (1978) *Mineral. Mag.* **42**, 533–63.
Mitchell, R. H. (1980) *Am. Mineral.* **65**, 45–54.
——and Platt, R. G. (1979) *Contrib. Mineral. Petrol.* **69**, 255–64.
Murthy, S. R. N. (1979) *Rec. Geol. Suv. India*, **112** (5), 15–35.
Naidu, P. J. R. (1963) *Min. Soc. Am. Sp. Paper*, **1**, 251–7.
Nash, W. P., and Wilkinson, J. F. G. (1970) *Contrib. Mineral. Petrol.* **25**, 241–69.
Parsone, I. (1979) *J. Petrol.* **20**, 653–94.
Powell, M., and Powell, R. (1974) *Contrib. Mineral. Petrol.* **48**, 249–63.
Ramanathan, S. (1954) *J. Madras Univ.* **24**, 315–33.
Schairer, J. F., and Yoder, H. S. (1960) *Am. J. Sci.* **258-A**, 273–83.
Smith, A. L., and Carmichael, I. S. E. (1969) *Am. Mineral.* **54**, 909–23.
Smith, D., and Lindsley, D. H. (1971) *Carnegie Inst. Washington Yearb.* **69**, 269–74.
Sørensen, H. (1974) *The Alkaline Rocks*, Wiley, London, 622 pp.
Stephenson, D. (1972) *Lithos*, **5**, 187–201.
Streckeisen, A. L. (1976) *Earth Sci. Rev.* **12**, 1–33.
Tilley, C. E. (1954) *Am. J. Sci.* **252**, 65–75.
Tuttle, O. F., and Smith, J. V. (1958) Ibid. **256**, 571–89.
Wells, P. R. A. (1977) *Contrib. Mineral. Petrol.* **42**, 129–39.
Wood, B. J., and Banno, S. (1973) Ibid. **42**, 109–24.

[*Manuscript received 8 July 1983; revised 20 October 1983*]